# Effects of edge potential on an armchair-graphene open boundary and nanoribbons

Chi-Hsuan Chiu and Chon-Saar Chu

*Department of Electrophysics, National Chiao Tung University, Hsinchu 30010, Taiwan, Republic of China*

(Received 17 December 2011; revised manuscript received 21 March 2012; published 23 April 2012)

Pseudospin flipping is found to be the key process leading to the formation of an edge-potential-induced edge state at an armchair-graphene open boundary and nanoribbons. At an open boundary, the edge potential $U_0$ is shown to turn on pseudospin-flipped (intravalley) scattering even though $U_0$ does not post an apparent breaking of the $AB$ site (basis atoms) symmetry. For a valley-polarized incident beam, the interference between the pseudospin-conserving (intervalley) and -nonconserving (intravalley) processes in the scattering state leads to a finite out-of-plane pseudospin density. This two-wave feature in the evanescent regime leads to the formation of the edge state. The physical origin of the edge state is different from that for the Tamm states in semiconductors. For an armchair-graphene nanoribbon with a gapless energy spectrum, applying $U_0$ to both edges opens up an energy gap. Both edge states and energy gap opening exhibit distinct features in nanoribbon conductance.

DOI: 10.1103/PhysRevB.85.155444 PACS number(s): 73.22.Pr, 72.80.Vp, 73.20.−r

## I. INTRODUCTION

Ever since the experimental separation of its sample,[1,2] graphene has become a fascinating paradigm for the germination of novel physical phenomena[3–8] and future applications in carbon-based nanoelectronics.[9–14] This is due to the fact that the low-energy physics in graphene is that of a two-dimensional massless Dirac particle,[1,15] and also to its striking material properties of high electronic mobility[16] and thermal conductivity.[17] The structure of graphene, a single honeycomb lattice layer of carbon atoms, has provided two additional twists, or degrees of freedom, to the Dirac physics. Pseudospin,[18–20] or the sublattice pseudospin, arises from the bipartite honeycomb lattice, which consists of two distinct triangular sublattices. Valley isospin[21–23] arises from two nonequivalent $K$ and $K'$ points (Dirac points) at the corners of the Brillouin zone. These have contributed to anomalous physical characteristics in phenomena such as Klein tunneling,[15,24,25] quantum Hall effects,[26,27] weak (anti)localization,[28–30] focusing of electron flow in a graphene $p$-$n$ junction,[31] and electron beam supercollimation.[18]

Edge states at a zigzag edge of graphene nanostructures has attracted an immense amount of attention recently.[32–50] These one-dimensional (1D) extended states, localized near the system edge, are zero-energy states of topological origin, and are the result of particle-hole symmetry.[35] The flatband nature of the edge states contributes to the large density of states in neutral zigzag graphene nanoribbons (GNRs) at the Fermi energy, and leads to localized magnetic structures at the zigzag edges.[33] Recent scanning tunneling spectroscopy measurements on chiral GNRs,[48] with a regular mixing of zigzag and armchair edges, reveals the presence of 1D GNR edge states.[48,49] There have been promising efforts to fabricate ideal GNRs with only zigzag or armchair edges.[51,52] The energy spectrum of the zigzag GNR is gapless because of the edge states.[5,33] On the other hand, the flatband feature of the edge states could support an energy gap when a Hubbard term for the on-site Coulomb repulsion is included.[33,46,48]

Edge potentials were invoked recently for the study of gap opening and gap modulation in the zigzag GNR.[45,47] For edge potentials applying along the GNR edges taking up either a $\delta$ profile[45] or a finite range profile across the GNR width,[47] the GNR energy spectrum opens up a gap when the applied potential is antisymmetric over the width of the GNR.[45,47] Meanwhile, the edge potential is also invoked to convert the flatband edge states into valley-dependent gapless edge states.[43] An on-site energy $U_0$ at the boundary is shown, when the $U_0$ magnitude is large enough, to suppress the hopping onto the outermost sites and to change the edge to that of a bearded edge.[43] In the presence of a bulk energy gap $\Delta$, due to a staggered sublattice potential, the continuous $U_0$ tuning of the edge-state dispersion relation between the zigzag-edge type and the bearded-edge type causes, at intermediate $U_0$ values, the conversion of the flatband edge states into gapless edge states that span the bulk energy gap.[43] The topological nature of these edge states derives from the fact that the states involve essentially only one valley ($K$ or $K'$), and that the topological charge[53] $\tilde{N}_3 = \frac{1}{2}\tau_z \mathrm{sgn}(\Delta)$ is nonzero for a valley.[43] Here $\tau_z = \pm$ is the valley index.

The armchair edge of graphene, on the other hand, has no edge states.[33–35,54] It is of interest then to consider the use of the edge potential for possible generation and tuning of the edge states. In this paper, we show that the edge potential $U_0$ at an open boundary does cause the formation of edge states, and the key is its turning on of the pseudospin-flipped (intravalley) scattering process. With this scattering process enabled, an incident wave in one valley will be reflected, at an armchair open boundary, into two scattered waves associated, separately, with $K$ and $K'$ valleys. The interference between the two scattered waves gives rise to out-of-plane pseudospin density, which is of interest in its own right. As for the edge-state formation, the two-wave feature is important because it opens up both evanescent waves, from $K$ and $K'$ valleys, for the construction of the edge-state wave function. Even though the two evanescent waves have different pseudospins, we show that the edge potential can provide the needed pseudospin rotation at the boundary for the edge-state boundary condition. Two interesting edge-state features are worth noticing here. The states are dispersive, and their formation does not require a finite threshold in $U_0$. The fact that the edge states are generated for arbitrary nonzero $U_0$ shows unequivocally that the physical origin is not Tamm-type[55]—the type of edge states induced, or trapped, by a sufficiently strong trapping potential at the

 

system boundary. Rather, the role of $U_0$ is to summon both evanescent waves for the formation of the edge states.

The effects of the edge potential on armchair GNRs are also explored in this work, with edge potentials that are symmetrically configured. Gap opening in the energy spectrum is obtained in addition to the aforementioned edge-state generation. To best illustrate the gap-opening features, we consider armchair GNRs that are gapless in their unperturbed energy spectrum by judiciously choosing the GNR widths.[33,38,39,56] Our finding shows that the energy gap (a global gap) is formed, at $\mathbf{k} = \mathbf{0}$, when an edgelike branch splits out of and in between GNR subbands. States in the edgelike branch have an edgelike spatial profile, except in the long wave-vector regime ($\mathbf{k} \approx \mathbf{0}$), where the spatial profile becomes bulklike. Interestingly, we can find an energy interval within which the edge states exist while the bulklike states do not. The characteristics in the GNR conductance associated with this energy interval are identified. As the propagation direction of the edge states is correlated with the pseudospin, it is expected that the edge states are insensitive to disorder. The scattering wave formulation which we have implemented in this work facilitates extraction of analytical results for better physical understanding. All our results compare well with direct numerical calculations.

This paper is organized as follows. In Sec. II, we present our scattering wave approach to an armchair-graphene open boundary in the presence of an edge potential $U_0$. The boundary condition is cast in a pseudospin scattering form most convenient for our discussion. For the scattering states, the out-of-plane pseudospin density is presented. For the edge states, an explicit form for the pseudospin rotation operator due to $U_0$ at the open boundary is presented. The edge-state dispersion relation is obtained numerically while its long-wavelength expression is obtained analytically. In Sec. III, we present our results for the armchair GNR due to a symmetrically configured edge potential. The finite-size effect on the edgelike branch and the gap opening in the GNR energy spectrum are presented. The effects of the edge potential on the armchair GNR conductance are also presented in Sec. IV. Finally, a conclusion is presented in Sec. V.

## II. ARMCHAIR GRAPHENE OPEN BOUNDARY

In this section, we present a scattering approach for the study of edge-potential effects on a armchair graphene open boundary. This approach allows us to extract, analytically, physical pictures such as the edge-potential-induced pseudospin scattering, the out-of-plane pseudospin density, and the edge-potential-induced edge states. In particular, the analytic expression for the edge-state dispersion relation in the long-wavelength regime shows that the edge states are generated for an arbitrary finite edge potential. This indicates that the edge state is not of Tamm-type. All the features found in this section will form the basis for the understanding of the edge-potential effects on the GNR in the next section.

### A. Basic model and a scattering approach

The conventions and notations that we adopt in this work are described briefly below in the introduction of our basic model. The tight-binding Hamiltonian[5] for a armchair graphene open

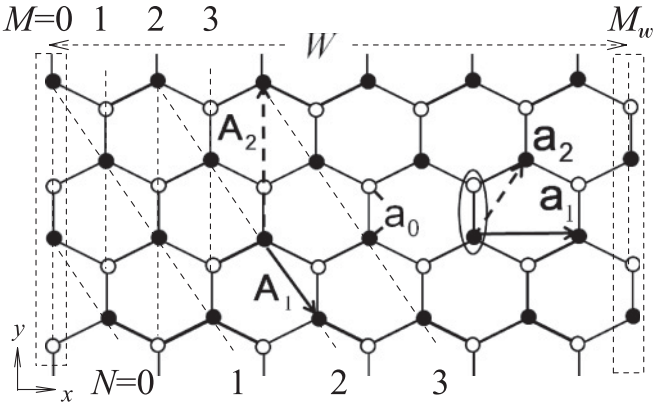


FIG. 1. Armchair GNR with unit-cell coordinates $M$ (vertical dotted lines) and $N$ (slanted dotted lines). Edges of the GNR are at $M = 0$ and $M_w$. Indicated are sites $A$ (•) and $B$ (○); Bravais lattice vectors $\mathbf{A}_1 = \mathbf{a}_1 - \mathbf{a}_2$ and $\mathbf{A}_2 = -\mathbf{a}_1 + 2\mathbf{a}_2$, where $\mathbf{a}_1 = 2a\hat{x}$ and $\mathbf{a}_2 = a\hat{x} + \sqrt{3}a\hat{y}$, and $a = \sqrt{3}\,a_0/2$, with C–C bond length $a_0 = 1.42$ Å.

boundary is given by

$$H = H_{\text{bulk}} + H_{\text{edge gate}}, \tag{1}$$

where

$$\begin{aligned} H_{\text{bulk}} &= -\gamma_0 \sum_{\langle i,j\rangle} \left(\hat{A}^\dagger_{\mathbf{R}_i} \hat{B}_{\mathbf{R}_j} + \hat{B}^\dagger_{\mathbf{R}_j} \hat{A}_{\mathbf{R}_i}\right), \\ H_{\text{edge gate}} &= \sum_i U_0 \left(\hat{A}^\dagger_{\mathbf{R}_i} \hat{A}_{\mathbf{R}_i} + \hat{B}^\dagger_{\mathbf{R}_i} \hat{B}_{\mathbf{R}_i}\right). \end{aligned} \tag{2}$$

The operators $\hat{A}^\dagger_{\mathbf{R}_i}$ and $\hat{A}_{\mathbf{R}_i}$ create and annihilate electrons at the $A$ site of the $i$th unit cell, respectively, with cell coordinates $(M_i, N_i)$ and cell location $\mathbf{R}_i = M_i\mathbf{A}_1 + N_i\mathbf{A}_2$, where $\mathbf{A}_1$ and $\mathbf{A}_2$ are Bravais lattice vectors. In terms of the more familiar Bravais lattice vectors $\mathbf{a}_1 = 2a\hat{x}$ and $\mathbf{a}_2 = a\hat{x} + \sqrt{3}a\hat{y}$ (see Fig. 1), we have $\mathbf{A}_1 = \mathbf{a}_1 - \mathbf{a}_2$ and $\mathbf{A}_2 = -\mathbf{a}_1 + 2\mathbf{a}_2$. Here $a = \sqrt{3}a_0/2$ and $a_0 = 1.42$ Å is the C–C bond length. We note that our choice of the cell coordinates $(M_i, N_i)$ is convenient for the armchair open boundary. Included in $\langle i, j\rangle$ are nearest-neighbor hoppings, with $\gamma_0 = 2.66$ eV. $H_{\text{bulk}}$ includes only $M_{i,j} \geqslant 0$ due to the $M = 0$ armchair boundary. The edge potential $H_{\text{edge gate}}$ applies an on-site energy $U_0$ to the $M_i = 0$ sites. In all the expressions that follow, whenever appropriate, units for energy, length, and wave vector are chosen to be $\gamma_0$, $a$, and $K_0 = 2\pi/(3a)$, respectively.

Scattering states at the armchair open boundary are constructed out of the Bloch states of graphene, albeit restricting the unit-cell summation in these Bloch states to $M \geqslant 0$. Specifically, Fig. 2 shows that the scattering state consists of an incident wave $|\Psi^{\text{B}}_{\mathbf{k}_\alpha}\rangle$, and intervalley and intravalley scattered waves $|\Psi^{\text{B}}_{\mathbf{k}_\beta}\rangle$ and $|\Psi^{\text{B}}_{\mathbf{k}_\gamma}\rangle$, respectively, given by

$$\left|\Psi^{(\text{sc})}_{\mathbf{k}_\alpha}\right\rangle = \left|\Psi^{\text{B}}_{\mathbf{k}_\alpha}\right\rangle + r_1\left|\Psi^{\text{B}}_{\mathbf{k}_\beta}\right\rangle + r_2\left|\Psi^{\text{B}}_{\mathbf{k}_\gamma}\right\rangle, \tag{3}$$

where $r_1$ ($r_2$) denotes the intervalley (intravalley) reflection coefficient. Here the Bloch states $|\Psi^{\text{B}}_{\mathbf{k}}\rangle$, given by

$$\left|\Psi^{\text{B}}_{\mathbf{k}}\right\rangle = \sum_{j,s} e^{i\mathbf{k}\cdot\mathbf{R}_j}\, C^{(s)}_{\mathbf{k}}\, |j,s\rangle\,, \tag{4}$$

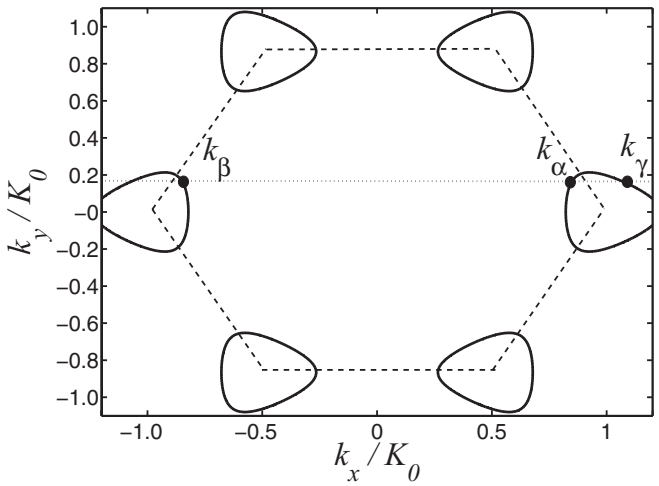


FIG. 2. States that involve reflection at the $M = 0$ open boundary in Fig. 1. Shown are the energy contour, the Brillouin zone boundary (dashed line), and valleys $K$ (at $K_0\hat{x}$) and $K'$ (at $-K_0\hat{x}$). The incident state is $\mathbf{k}_\alpha$ and the intervalley (intravalley) reflected state is $\mathbf{k}_\beta$ ($\mathbf{k}_\gamma$). The index for the left- (right-) going state is $\xi = 1(\bar{1})$. The index for the $K$ ($K'$) valley is $\eta = 1$ ($\bar{1}$). Here, $\alpha = (\xi,\eta) = (1,1)$, $\beta = (\bar{\xi},\bar{\eta})$, and $\gamma = (\bar{\xi},\eta)$.

sum over the unit-cell index $j$ up to the open boundary ($M_j \geqslant 0$), and over the $A$ ($B$) site index $s = 1$ (2). This scattering state approach has an advantage over the direct numerical approach in that the asymptotic ($M \gg 1$) boundary condition is already taken care of by the Bloch states, and the scattering problem is reduced to the finding of only two reflection coefficients.

To set the stage for the pseudospin scattering processes in the next subsection, we provide the explicit form of the pseudospinor in the following:

$$\left(C_{\mathbf{k}}^{(1)}, C_{\mathbf{k}}^{(2)}\right)^T = N_{\mathbf{k}}\left(1, \pm\sqrt{H_{\mathbf{k}}\tilde{H}_{\mathbf{k}}}/H_{\mathbf{k}}\right)^T. \tag{5}$$

Here $N_{\mathbf{k}}$ is the normalization constant for the pseudospinor, and $\pm$ is for the conduction (valence) band. Furthermore, $H_{\mathbf{k}} = -\gamma_0[1 + 2e^{-i\sqrt{3}k_y a}\cos(k_x a)]$, whereas $\tilde{H}_{\mathbf{k}} = -\gamma_0[1 + 2e^{i\sqrt{3}k_y a}\cos(k_x a)]$. For real wave vector $\mathbf{k}$, $\tilde{H}_{\mathbf{k}} = H_{\mathbf{k}}^*$, so that $C_{\mathbf{k}}^{(2)} = H_{\mathbf{k}}^*/(\sqrt{2}\,|H_{\mathbf{k}}|)$ carries the phase of $H_{\mathbf{k}}^*$, and the pseudospin orientation is in-plane.

In contrast, the pseudospin orientation becomes out-of-plane when $\mathbf{k}$ is complex. For our purposes here, $k_x$ is determined from

$$\cos(k_x a) = -\frac{1}{2}\cos(\sqrt{3}k_y a) + \frac{\xi\eta}{2}\sqrt{E^2 - \sin^2(\sqrt{3}k_y a)} \tag{6}$$

for a given $k_y$ and energy $E$. A complex $k_x$ is conveniently cast in the form $k_x = \eta\kappa_r - i\xi\kappa_i$, where $\kappa_r$ and $\kappa_i$ are positive, and $\eta = 1$ ($\bar{1}$) denotes the $K$ ($K'$) valley, while $\xi = 1$ ($\bar{1}$) denotes the left- (right-) going state. We have $k_{\beta x} = -k_{\alpha x}$ for intervalley reflection and $k_{\gamma x} = k_{\alpha x}^*$ for intravalley reflection. Since both $H_{\mathbf{k}}$ and $\tilde{H}_{\mathbf{k}}$ are even in $k_x$, regardless of whether $k_x$ is real or complex, the pseudospins for $k_{\alpha x}$ and $k_{\beta x}$ are the same, but they are different from the pseudospin for $k_{\gamma x}$.

It is known[5] that scattering at a pristine armchair graphene open boundary involves only intervalley reflection where pseudospin is conserved. Applying an edge potential $H_{\text{edge gate}}$ that affects equally the $A$ and $B$ site potentials in a unit cell seems not to have broken the equal preference of staying in either site, and thus it seems to be pseudospin-conserving. Our finding in the next subsection, however, shows the contrary.

### B. Edge-potential-induced pseudospin scattering

In this subsection, we demonstrate the physical origin of pseudospin flipping due to the edge potential $H_{\text{edge gate}}$. Insight in this regard is obtained from the unit-cell recurrence relation. By substituting Eqs. (3) and (4) into Eq. (1) and focusing upon the coefficient of the term $e^{ik_y R_{jy}}$, the recurrence relations are obtained as

$$(-U_0 + \sigma_x)\,V_0 + \mathbf{T}V_1 = -EV_0, \tag{7a}$$

$$\mathbf{T}V_{M-1} + \sigma_x V_M + \mathbf{T}V_{M+1} = -EV_M, \tag{7b}$$

where $V_M = (\phi_M^{(1)}, \phi_M^{(2)})^T$ is the wave-function amplitude at the $M$th unit cell, with

$$\phi_M^{(s)} = e^{ik_{\alpha x}Ma}C_{\mathbf{k}_\alpha}^{(s)} + r_1 e^{ik_{\beta x}Ma}C_{\mathbf{k}_\beta}^{(s)} + r_2 e^{ik_{\gamma x}Ma}C_{\mathbf{k}_\gamma}^{(s)}. \tag{8}$$

Equation (7b) is obtained from the coefficients at the $M$th unit cell for $M > 0$ and energy $E$. Terms involving $\mathbf{T}$ and $\sigma_x$ are from intercell and intracell hopping, respectively. Actually, the same equation gives the bulk recurrence relation for the Bloch states. On the other hand, Eq. (7a) carries the sole effect of the edge potential via the term $-U_0 V_0$. No unit cell of smaller $M$ exists to contribute to the hopping, and the negative sign on $U_0$ follows from our sign convention for the hopping coefficient $-\gamma_0$. The hopping matrix $\mathbf{T}$ is given by

$$\mathbf{T} = \begin{pmatrix} 0 & e^{-i\sqrt{3}k_y a} \\ e^{i\sqrt{3}k_y a} & 0 \end{pmatrix}. \tag{9}$$

Equation (7) is cast into a compact form by borrowing a symbol $V_{-1}$ from, mathematically, the bulk recurrence relation in Eq. (7b) to $M = 0$, and substituting it into Eq. (7a), to give

$$U_0 V_0 + \mathbf{T}V_{-1} = 0. \tag{10}$$

The expression for $V_{-1}$ is given by Eq. (8), and Eq. (10) is expanded to give

$$\begin{pmatrix} U_0 C_{\mathbf{k}_\beta}^{(1)} + C_{\mathbf{k}_\beta}^{(2)} e^{-i\mathbf{k}_\beta\cdot\mathbf{a}_2} & U_0 C_{\mathbf{k}_\gamma}^{(1)} + C_{\mathbf{k}_\gamma}^{(2)} e^{-i\mathbf{k}_\gamma\cdot\mathbf{a}_2} \\ U_0 C_{\mathbf{k}_\beta}^{(2)} + C_{\mathbf{k}_\beta}^{(1)} e^{-i\mathbf{k}_\beta\cdot(\mathbf{a}_1-\mathbf{a}_2)} & U_0 C_{\mathbf{k}_\gamma}^{(2)} + C_{\mathbf{k}_\gamma}^{(1)} e^{-i\mathbf{k}_\gamma\cdot(\mathbf{a}_1-\mathbf{a}_2)} \end{pmatrix} \begin{pmatrix} r_1 \\ r_2 \end{pmatrix} = -\begin{pmatrix} U_0 C_{\mathbf{k}_\alpha}^{(1)} + C_{\mathbf{k}_\alpha}^{(2)} e^{-i\mathbf{k}_\alpha\cdot\mathbf{a}_2} \\ U_0 C_{\mathbf{k}_\alpha}^{(2)} + C_{\mathbf{k}_\alpha}^{(1)} e^{-i\mathbf{k}_\alpha\cdot(\mathbf{a}_1-\mathbf{a}_2)} \end{pmatrix}. \tag{11}$$

Rearranging into a form more convenient for our discussion on the reflection coefficients, we get

$$\begin{pmatrix} U_0 C_{\mathbf{k}_\beta}^{(1)} + C_{\mathbf{k}_\beta}^{(2)} e^{-i\mathbf{k}_\beta\cdot\mathbf{a}_2} \\ U_0 C_{\mathbf{k}_\beta}^{(2)} + C_{\mathbf{k}_\beta}^{(1)} e^{-i\mathbf{k}_\beta\cdot(\mathbf{a}_1-\mathbf{a}_2)} \end{pmatrix} r_1 + \begin{pmatrix} U_0 C_{\mathbf{k}_\gamma}^{(1)} + C_{\mathbf{k}_\gamma}^{(2)} e^{-i\mathbf{k}_\gamma\cdot\mathbf{a}_2} \\ U_0 C_{\mathbf{k}_\gamma}^{(2)} + C_{\mathbf{k}_\gamma}^{(1)} e^{-i\mathbf{k}_\gamma\cdot(\mathbf{a}_1-\mathbf{a}_2)} \end{pmatrix} r_2 = -\begin{pmatrix} U_0 C_{\mathbf{k}_\alpha}^{(1)} + C_{\mathbf{k}_\alpha}^{(2)} e^{-i\mathbf{k}_\alpha\cdot\mathbf{a}_2} \\ U_0 C_{\mathbf{k}_\alpha}^{(2)} + C_{\mathbf{k}_\alpha}^{(1)} e^{-i\mathbf{k}_\alpha\cdot(\mathbf{a}_1-\mathbf{a}_2)} \end{pmatrix}. \tag{12}$$

Equations (11) and (12) are two key relations in this work.

Taking $U_0 = 0$ in Eq. (12), we see that $r_1 = -e^{-2ik_{\alpha x}a}$ and $r_2 = 0$. This results from the fact that the $\mathbf{k}_\alpha$ and $\mathbf{k}_\beta$ states have the same pseudospin and the $\mathbf{k}_\gamma$ state has a different pseudospin. Furthermore, $(\mathbf{k}_\beta - \mathbf{k}_\alpha)\cdot\mathbf{a}_2 = (\mathbf{k}_\beta - \mathbf{k}_\alpha)\cdot(\mathbf{a}_1 - \mathbf{a}_2) = -2k_{\alpha x}a$. Pseudospin is conserved. Taking $U_0 \neq 0$, however, has effectively brought about other pseudospins. In fact, the on-site nature of $U_0$ has kept intact the pseudospins of the associated terms in Eq. (12), whereas the other terms have their $C_{\mathbf{k}}^{(s)}$ coefficients inverted due to their hopping origin. Thus $r_2$ can no longer remain zero, and pseudospin flipped reflection is invoked. It is clear that the turning on of the pseudospin flipped reflection does not require a threshold $U_0$, but rather a nonzero $U_0$.

A comment on our seemingly surprising result, namely that the edge potential $H_{\text{edge gate}}$ affects equally the $A$ and $B$ sites on the open boundary and can open up pseudospin flipped reflection, is in order here. Equation (12) clearly shows that pseudospins associated with $U_0$ have their in-plane nature kept intact. This is expected. What one might overlook, however, is that $U_0$ can still bring about pseudospins other than the incident one. Equation (12) shows that this is achieved by way of relative phases between the two components of a pseudospin.

### C. Out-of-plane pseudospin density

As $U_0$ opens up a pseudospin flipped channel, interference between the pseudospins of the reflected waves will occur. Since the pseudospins are in-plane for real $\mathbf{k}$, the interference will lead to out-of-plane pseudospin.

In this subsection, we present the out-of-plane pseudospin polarization $\mathcal{PP}_{z\eta}$ in the vicinity of the $M = 0$ boundary. Incident states propagating along $+y$ with energy within $\Delta E$ and from one valley (index $\eta$) are included. The density $n_{s\eta}(E, M_j)$ in the $j$th unit cell is

$$n_{s\eta}(E, M_j) = \sum_{\mathbf{k}_\alpha}{}' \left|\langle j,s|\Psi_{\mathbf{k}_\alpha}^{(\text{sc})}\rangle\right|^2, \tag{13}$$

where the primed summation has restricted the energy to the range $E \leqslant E(\mathbf{k}_\alpha) \leqslant E + \Delta E$, and $k_{\alpha y} > 0$. Here $s$ refers to the $A$ ($B$) sites, and $\alpha = (1,\eta)$ for incident $\mathbf{k}_\alpha$. Equation (13), or $n_{s\eta}$, depends on $M_j$ but not on $N_j$, as it should. The pseudospin polarization, as defined by

$$\mathcal{PP}_{z\eta} \equiv \frac{n_{A\eta} - n_{B\eta}}{n_{A\eta} + n_{B\eta}}, \tag{14}$$

is presented in Fig. 3, where $M$ is used instead of $M_j$. The decay of $\mathcal{PP}_{z\eta}$ with $M$ is due to the spread in the wave vector $\Delta k_x(E)$, the range of which is subjected to the restrictions imposed by the summation. This leads to a decrease in the decay length with increasing $E$, as is seen in Figs. 3(a)–3(d). Meanwhile, $\mathcal{PP}_{z\eta}$ changes sign as its valley-index $\eta$ is changed, or as the incident wave vectors are changed, from $k_y > 0$ to $k_y < 0$. Finally, the magnitude of $\mathcal{PP}_{z\eta}$ increases with $U_0$, as is demonstrated in comparing Figs. 3(a) and 3(c).

This out-of-plane pseudospin distribution can be realized in the presence of a valley-polarized incident beam. The recent development in valleytronics and, in particular, proposals on valley-filter[21,23] and valley-polarized electron beams[22] are, thus, of direct relevance to this work.

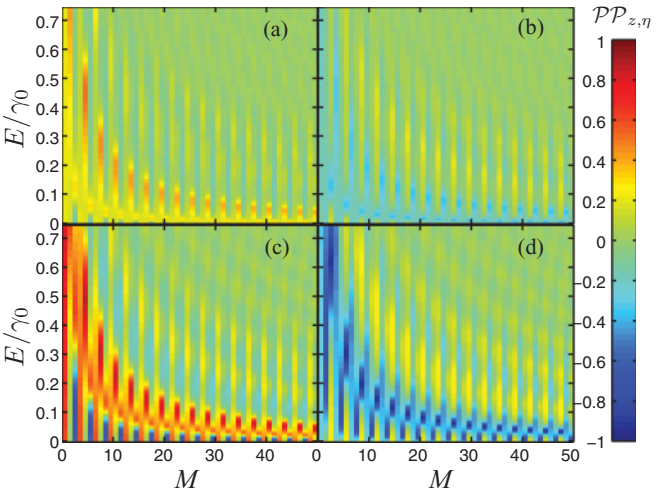


FIG. 3. (Color online) Contour plot of valley-dependent pseudospin polarization $\mathcal{PP}_{z\eta}$ against unit-cell location $M$ and energy $E$. Edge potential $U_0 = 0.2$ in (a),(b) and $U_0 = 1.0$ in (c),(d). Contribution from $K$ valley ($\eta = 1$) is shown in (a) and (c), and from $K'$ valley ($\eta = -1$) is in (b) and (d). States within $\Delta E = 5 \times 10^{-3}$ are included. The sign of $\mathcal{PP}_{z\eta}$ reverses with $\eta$ but the magnitude remains the same.

### D. Edge-potential-induced edge states

In this subsection, we turn our attention to edge states, and we identify the key physical process that enables their formation. The pseudospin of these edge states, however, does not have an out-of-plane component. We will explain the reason for this in our analytical analysis.

Starting with Eq. (3), but without an incident component $|\Psi_{\mathbf{k}_\alpha}^{\text{B}}\rangle$, we look for edge-state energy $E_{\text{ed}}$ for a given $k_y$ in the complex $k_x$ regime. Already, Eq. (11) has provided the basis for the numerical calculation of $E_{\text{ed}}$. This is from the zeros of the determinant of the matrix on the left-hand side of Eq. (11). The case for positive $U_0$'s is illustrated in Fig. 4. Turning on $U_0$, an edge state branch is formed out of the bulk state continuum (gray area) on the valence-band side. Increasing $U_0$ pushes the branch away from the continuum. Near $U_0 = 1$, the edge-state branch has a zero slope near a Dirac cone. Beyond $U_0 = 1$, the slope in the long-wavelength regime increases monotonically with $U_0$ and approaches that of the continuum on the conduction-band side. A change in the sign of $U_0$ simply changes the sign of $E_{\text{ed}}$.

A number of interesting features about these edge states are in order here. These edge states are obtained without opening a gap in the bulk state continuum. The dispersion relations $E_{\text{ed}}(k_y)$ for all $U_0$ start and end at Dirac cones. These include cases when $U_0$ is arbitrarily small but nonzero. There is no threshold $U_0$, and this, in turn, assures us that the physics for this edge-state formation is not Tamm-type.[55] In fact, the edge-state formation is enabled by the opening up of the pseudospin flipped channel, and by a pseudospin rotation at the boundary. This pseudospin rotation analysis will be discussed in the last part of this subsection.

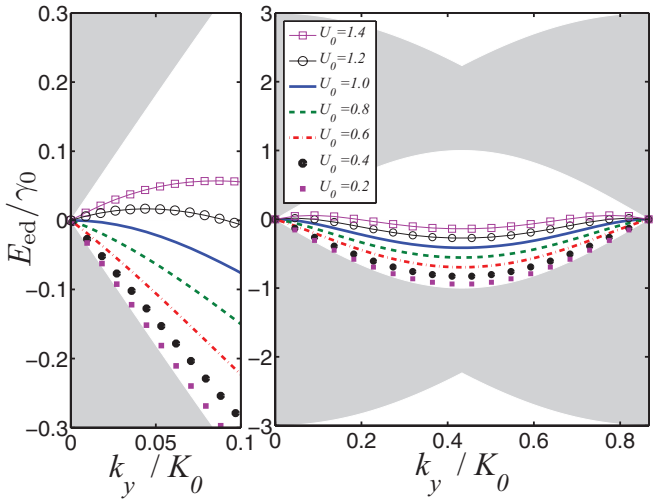


FIG. 4. (Color online) Edge-state dispersion relations induced by $U_0$ at an armchair open boundary are shown for $U_0 = 1.4$ (open square), 1.2 (open circle), 1 (solid curve), 0.8 (dashed curve), 0.6 (dashed-dotted curve), 0.4 (solid circle), and 0.2 (solid square). Gray areas depict the bulk electron continuum spectrum. Right panel shows a $k_y$ range that includes two Dirac cones. Left panel shows a smaller $k_y$ range.

An analytical expression for $E_{\rm ed}(k_y)$ is derived near the Dirac cone, in the long-wavelength regime $k_y a_{2y} \ll 1$. This complements our numerical results given above for a better understanding. Assuming the form $E_{\rm ed} = \alpha_1(U_0)|q_y|$, where $|q_y| = |k_y|a_{2y} \ll 1$, and the coefficient $\alpha_1(U_0)$, the $U_0$ it depends on is not necessarily small. We obtain, from Eq. (6), $k_x^\eta = (\eta K + \Delta k_{xr}^\eta) + i\Delta k_{xi}$. Here $\eta = 1$ and $-1$ correspond to cases for $\mathbf{k}_\gamma$ and $\mathbf{k}_\beta$, respectively. To lowest order in $q_y$, we have

$$\begin{aligned} \Delta k_{xi} &= \frac{1}{\sqrt{3}}\sqrt{1-\alpha_1^2}|q_y| \equiv G(U_0)|q_y|, \\ \Delta k_{xr}^\eta &= -\frac{\eta}{2\sqrt{3}}[1+G^2(U_0)]q_y^2, \end{aligned} \tag{15}$$

where $G(U_0) = \frac{1}{\sqrt{3}}\sqrt{1-\alpha_1^2(U_0)}$. The coefficient $\alpha_1(U_0)$ is derived from requiring the determinant of the matrix in Eq. (11) to be zero. Using the relation $C_{\mathbf{k}}^{(2)}/C_{\mathbf{k}}^{(1)} = E_{\rm ed}/H_{\mathbf{k}}$, we obtain, up to the second order in $q_y$,

$$\frac{-U_0\alpha_1}{1-U_0^2} = \sqrt{\frac{1-\alpha_1^2}{3}}. \tag{16}$$

Subsequently, in the $k_y a_{2y} \ll 1$ regime, we obtain

$$E_{\rm ed} \approx {\rm sgn}(U_0)\frac{\sqrt{3}\left(U_0^2-1\right)}{\sqrt{1+U_0^2+U_0^4}}|k_y|a. \tag{17}$$

This is another key expression, which is valid to all orders in $U_0$.

The boundary condition, given by Eq. (12), must be in a pseudospin rotation form at the energy $E_{\rm ed}(k_y)$, which connects pseudospins of the $\mathbf{k}_\beta$ and $\mathbf{k}_\gamma$ states. From Eq. (12), and dropping terms associated with $\mathbf{k}_\alpha$, we have

$$D_\beta \begin{pmatrix} C_{\mathbf{k}_\beta}^{(1)} \\ C_{\mathbf{k}_\beta}^{(2)} \end{pmatrix} r_1 + D_\gamma \begin{pmatrix} C_{\mathbf{k}_\gamma}^{(1)} \\ C_{\mathbf{k}_\gamma}^{(2)} \end{pmatrix} r_2 = 0, \tag{18}$$

where $D_\beta = [U_0 + e^{-ik_{\beta x}a}\mathbf{T}]$ and $D_\gamma = [U_0 + e^{-ik_{\gamma x}a}\mathbf{T}]$. This amounts to requiring $\mathscr{D} \equiv -(r_2/r_1)D_\beta{}^{-1}D_\gamma$ to rotate $\mathbf{k}_\gamma$'s pseudospin to that of the $\mathbf{k}_\beta$ state. The explicit form of $\mathscr{D}$ is

$$\mathscr{D} = -\frac{r_2/r_1}{\Lambda}\begin{pmatrix} 1-U_0^2e^{-2k_{xi}a} & ie^{-i\sqrt{3}k_y a}[2U_0e^{-k_{xi}a}\sin(k_{xr}a)] \\ ie^{i\sqrt{3}k_y a}[2U_0e^{-k_{xi}a}\sin(k_{xr}a)] & 1-U_0^2e^{-2k_{xi}a} \end{pmatrix}, \tag{19}$$

where $k_{xr} = {\rm Re}\,k_{\gamma x}$, $k_{xi} = {\rm Im}\,k_{\gamma x}$, and $\Lambda = U_0^2e^{-2k_{xi}a} - e^{i2k_{xr}a}$. The unimodular property of $\mathscr{D}$ has $\mathscr{D}(1,1) = \mathscr{D}^*(2,2)$, or $r_2/r_1\Lambda$ a real number, and the property $|\mathscr{D}(1,1)|^2 + |\mathscr{D}(1,2)|^2 = 1$ leads to $|r_2/r_1| = 1$, which is checked with our numerical results. We have thus demonstrated that the formation of the edge state requires the pseudospin rotation to satisfy a particular condition at the boundary, namely $|r_2/r_1| = 1$.

On the other hand, $\mathscr{D}$ can be expressed in terms of the orientation angles of the two pseudospins. The pseudospin states of $\mathbf{k}_\beta$ and $\mathbf{k}_\gamma$ are of the form $[\cos(\theta/2), \sin(\theta/2)e^{i\phi}]^T$ and $[\sin(\theta/2), \cos(\theta/2)e^{i\phi}]^T$, where $\theta$ and $\phi$ are real numbers representing the pseudospins' angles of orientation. As an operator that rotates an angle $\pi - 2\theta$ about an axis along $[\cos(\phi)\hat{x} + \sin(\phi)\hat{y}] \times \hat{z}$, we must also have

$$\mathscr{D} = \begin{pmatrix} \sin\theta & e^{-i\phi}\cos\theta \\ -e^{i\phi}\cos\theta & \sin\theta \end{pmatrix}. \tag{20}$$

Comparing Eqs. (19) and (20), we have

$$\sin\theta = -\left(1-U_0^2e^{-2k_{xi}a}\right)/|\Lambda|, \tag{21a}$$

$$\cos\theta = -(2U_0e^{-k_{xi}a}\sin k_{xr}a)/|\Lambda|, \tag{21b}$$

$$e^{-i\phi} = ie^{-i\sqrt{3}k_y a}. \tag{21c}$$

The relation $|r_2/r_1| = 1$ that the edge states are required to obey has important bearings on their pseudospin. Expressed in terms of $\theta$ and $\phi$, the edge-state wave function $\Psi_{\rm ed}(M)$ at the $M$th unit cell, in pseudospin form, is given by

$$\Psi_{\rm ed}(M) = r_1\, e^{ik_{\beta x}Ma}\begin{pmatrix} \cos(\theta/2) \\ \sin(\theta/2)e^{i\phi} \end{pmatrix} + r_2\, e^{ik_{\gamma x}Ma}\begin{pmatrix} \sin(\theta/2) \\ \cos(\theta/2)e^{i\phi} \end{pmatrix},$$

from which we calculate the pseudospin polarization $\mathcal{PP}_{z,\mathrm{ed}}(M)$, and we obtain

$$\mathcal{PP}_{z,\mathrm{ed}}(M) \equiv \frac{\Psi_{\mathrm{ed}}^{\dagger}\,\sigma_z\,\Psi_{\mathrm{ed}}}{\Psi_{\mathrm{ed}}^{\dagger}\Psi_{\mathrm{ed}}} = 0. \tag{22}$$

The fact that $\mathcal{PP}_{z,\mathrm{ed}}$ is zero in Eq. (22) is clearly seen from $\Psi_{\mathrm{ed}}^{\dagger}\,\sigma_z\Psi_{\mathrm{ed}} = e^{-2\,\mathrm{Im}(k_{\beta x})Ma}\cos\theta\,(|r_1|^2 - |r_2|^2)$, which vanishes when $|r_2/r_1| = 1$.

## III. ARMCHAIR-GRAPHENE NANORIBBON

In this section, the effects of the edge potential on armchair GNR are studied. The scattering approach we invoked in the previous section is applied here, and simplifications in both the formulation and subsequent analysis are achieved. Features studied include the generation of edge states, their hybridization due to finite ribbon widths, band-gap modulation, and pseudospin characteristics. An expression for the band gap, up to second order in $U_0$, is obtained. In addition, an energy window in the electron spectrum is found within which the states are all edge states.

### A. Formulation with scattering approach

The armchair GNR (see Fig. 1) has edges at $M = 0$ and $M_w$, and a total number of sites $W = M_w + 1$ across the width. The edge potential $H_{\text{edge gate}}$ in Eq. (2) now has $M_i = 0$ and $M_w$. Following Eq. (3), the GNR eigenstates $|\Psi^{(\mathrm{NR})}\rangle$ consist of four Bloch states, all of the form given by Eq. (4) but with the sum over the unit-cell index $j$ restricted to the interval $0 \leqslant M_j \leqslant M_w$. For convenience of presentation, we label Bloch states that correspond to the $K$ valley as $A$ and $B$, with their $(\xi,\eta) = (\bar{1},1)$ and $(1,1)$, respectively. Bloch states that correspond to the $K'$ valley are labeled $C$ and $D$, with their $(\xi,\eta) = (1,\bar{1})$ and $(\bar{1},\bar{1})$, respectively. For a given $k_y$ and energy $E$, we have

$$|\Psi^{(\mathrm{NR})}\rangle = \mathcal{A}\big|\Psi^{\mathrm{B}}_{\mathbf{k}_\mathrm{A}}\big\rangle + \mathcal{B}\big|\Psi^{\mathrm{B}}_{\mathbf{k}_\mathrm{B}}\big\rangle + \mathcal{C}\big|\Psi^{\mathrm{B}}_{\mathbf{k}_\mathrm{C}}\big\rangle + \mathcal{D}\big|\Psi^{\mathrm{B}}_{\mathbf{k}_\mathrm{D}}\big\rangle. \tag{23}$$

These coefficients are connected by reflections at the boundaries, given by

$$\begin{pmatrix} -1 & r_{\mathrm{AB}} & r_{\mathrm{AC}} & 0 \\ \tilde{r}_{\mathrm{BA}} & -1 & 0 & \tilde{r}_{\mathrm{BD}} \\ \tilde{r}_{\mathrm{CA}} & 0 & -1 & \tilde{r}_{\mathrm{CD}} \\ 0 & r_{\mathrm{DB}} & r_{\mathrm{DC}} & -1 \end{pmatrix} \begin{pmatrix} \mathcal{A} \\ \mathcal{B} \\ \mathcal{C} \\ \mathcal{D} \end{pmatrix} = 0. \tag{24}$$

Here $r_{\nu\mu}$ denotes the reflection coefficient at the $M = 0$ edge from Bloch states $\mu$ to $\nu$, and $\tilde{r}_{\nu\mu}$ denotes reflection at the $M = M_w$ edge.

In this work, the applied edge potential is symmetric with respect to the center of the ribbon. Thus Eq. (24) can be simplified further by exploiting the parity symmetry. This is carried out by replacing $R_{jx}$ by $R_{jx} - M_w a/2$ in the unit-cell summation of $|\Psi^{\mathrm{B}}_{\mathbf{k}_y}\rangle$. The parity of the nanoribbon eigenstate $|\Psi^{(\mathrm{NR})}\rangle$ is imposed by the relations $\mathcal{C} = \pm\mathcal{A}$ and $\mathcal{B} = \pm\mathcal{D}$, where the upper (lower) sign corresponds to even (odd) parity. Equation (24) is reduced to

$$\begin{pmatrix} 1 \mp r_{\mathrm{AC}} & \mp r_{\mathrm{AB}} \\ \mp r_{\mathrm{DC}} & 1 \mp r_{\mathrm{DB}} \end{pmatrix} \begin{pmatrix} \mathcal{C} \\ \mathcal{B} \end{pmatrix} = 0. \tag{25}$$

The energy spectrum for each parity is determined separately, according to Eq. (25). Level anticrossing thus occurs only between states of the same parity because the edge potential preserves the symmetry. For our convenience below, the reflections from states {B,C} into states {A,D} are represented by the reflection of state $\alpha = (\xi = 1,\eta)$ into states $\beta = (\bar{\xi},\bar{\eta})$ and $\gamma = (\bar{\xi},\eta)$. The reflection coefficients in Eq. (25) are then labeled as $r_{1\alpha}$ and $r_{2\alpha}$, with subscript 1 (2) denoting intervalley (intravalley) reflection. These coefficients are obtained, following a similar procedure that leads to Eq. (11), as

$$\begin{pmatrix} e^{-ik_{\beta x}M_w a/2}\big[U_0\,C^{(1)}_{\mathbf{k}_\beta} + C^{(2)}_{\mathbf{k}_\beta}e^{-i\mathbf{k}_\beta\cdot\mathbf{a}_2}\big] & e^{-ik_{\gamma x}M_w a/2}\big[U_0\,C^{(1)}_{\mathbf{k}_\gamma} + C^{(2)}_{\mathbf{k}_\gamma}e^{-i\mathbf{k}_\gamma\cdot\mathbf{a}_2}\big] \\ e^{-ik_{\beta x}M_w a/2}\big[U_0\,C^{(2)}_{\mathbf{k}_\beta} + C^{(1)}_{\mathbf{k}_\beta}e^{-i\mathbf{k}_\beta\cdot(\mathbf{a}_1-\mathbf{a}_2)}\big] & e^{-ik_{\gamma x}M_w a/2}\big[U_0\,C^{(2)}_{\mathbf{k}_\gamma} + C^{(1)}_{\mathbf{k}_\gamma}e^{-i\mathbf{k}_\gamma\cdot(\mathbf{a}_1-\mathbf{a}_2)}\big] \end{pmatrix} \begin{pmatrix} r_{1\alpha} \\ r_{2\alpha} \end{pmatrix}$$
$$= \begin{pmatrix} e^{-ik_{\alpha x}M_w a/2}\big[U_0 C^{(1)}_{\mathbf{k}_\alpha} + C^{(2)}_{\mathbf{k}_\alpha}\,e^{-i\mathbf{k}_\alpha\cdot\mathbf{a}_2}\big] \\ e^{-ik_{\alpha x}M_w a/2}\big[U_0 C^{(2)}_{\mathbf{k}_\alpha} + C^{(1)}_{\mathbf{k}_\alpha}\,e^{-i\mathbf{k}_\alpha\cdot(\mathbf{a}_1-\mathbf{a}_2)}\big] \end{pmatrix}. \tag{26}$$

Numerical results from this scattering approach compare well with exact diagonalization results. Moreover, Eqs. (26) and (25) provide a useful starting point for the derivation of the edge-potential-induced gap modulation, to be presented in a later subsection.

### B. GNR energy spectrum

In the following, we present the energy spectrum of armchair GNR under the effect of edge potentials. To better illustrate the edge-potential-induced gap-opening features, the GNRs considered here are of the type $W = 3p + 2$ for nonnegative integer $p$, such that their unperturbed energy spectra are gapless.[33,38,39,56] Figure 5 presents the energy spectrum of an armchair GNR for $U_0 = 1$ and $W = 80$ and 41, respectively, in Figs. 5(a) and 5(b). The same spectrum occurs around another Dirac cone at $k_y = \sqrt{3}K_0/2$. Edge-state branches are the isolated branches separated from the GNR subbands. The GNR subbands open up an energy interval between them, at the Dirac cone, leaving room for the edge-state branches to develop. This is seen more clearly in Figs. 5(a′) and 5(b′), where smaller $k_y$ ranges are shown. The gray areas are the continuum spectrum for the bulk graphene, given by Eq. (6). States with energy $E(k_y)$ that falls outside the gray area should have their wave function exhibiting exponential behavior. Guided by this, the GNR subbands and the edge-state branches

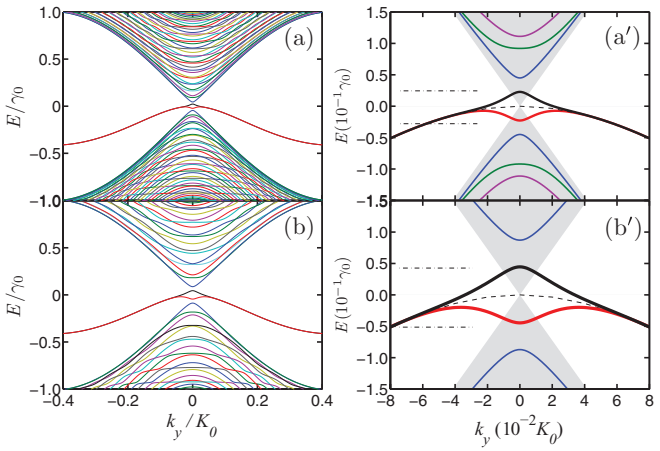


FIG. 5. (Color online) Energy spectrum of armchair GNR for $U_0 = 1$, and $W = 80$ in (a) and 41 in (b). Smaller $k_y$ ranges are shown in (a′) and (b′), where gray areas are the continuum spectrum for the bulk graphene. Two branches outside the gray areas are edge-state branches: odd (even) parity for the upper (lower) branch. Dotted curve between the edge-state branches is that for a single open boundary. Horizontal (dotted-dashed) line segments in (a′) and (b′) denote energies to be considered in Fig. 6.

are easily identified. Furthermore, the edge states have two branches with the upper (lower) branch having odd (even) parity. This results from hybridizations between edge states on the two GNR edges. The fact that the edge-state branch for an open boundary, denoted by the dotted curve, is centrally positioned in energy between the two edge-state branches demonstrates a degenerate splitting feature, and it indicates that the edge states are pretty well formed. When the two branches overlap in energy, for sufficiently large $k_y$, the edge states on the two GNR edges become decoupled. It is worth pointing out that when the small $k_y$ region of the edge-state branches falls within the gray area, their spatial profiles $|\Psi_{A/B}^{(NR)}|^2$, on the A or B sites, are expected to exhibit bulklike characteristics. This is found in Fig. 6. When the edge-state branches overlap, linear superpositions of the even- and odd-parity wave functions produce edge-state wave functions $\Psi_{R\,(L)}^{(NR)}$ that localize on the right (left) edges. These are shown in Figs. 6(a) and 6(b) for, respectively, the cases of $E = -0.03$, and $-0.05$.

Another important indication shown in Fig. 6 concerns the out-of-plane pseudospin for the edge states. The $|\Psi_A^{(NR)}|^2$ and $|\Psi_B^{(NR)}|^2$ curves fall exactly on top of one another in Fig. 6. This implies that the out-of-plane pseudospin vanishes for the edge states. Furthermore, the out-of-plane pseudospins of the GNR subbands are also found to be zero. We think that this is due to the highly symmetric alignment of the GNR edges. For less symmetric graphene boundary configurations, however, the edge-potential-induced out-of-plane pseudospin feature is expected to manifest near an armchair open boundary. This is left for further investigation.

We present in Fig. 7 the evolution of the two edge-state branches with the increase of $U_0$. For positive $U_0$, the edge-state branches are being drawn from the two highest GNR valence subbands. Meanwhile, an energy gap is formed which is increasing with $U_0$, and is indicated by $\Delta_p$ in Fig. 7(c). The gap is formed between two odd-parity branches, namely the GNR subband, denoted by $E_{bulk}^{odd}$, and the edge-state branch, denoted by $E_{edge}^{odd}$. On the other hand, there is an energy window in the spectrum that consists of only edge states. For example, in Fig. 7(c), the energy window, bounded by the $k_y = 0$ edge-state branch (even parity) and its neighboring GNR subband, on the lower energy side, is of the order of $0.02\gamma_0$.

### C. Edge-potential-induced gap modulation

In this subsection, the edge-potential-induced energy gap $\Delta_p(U_0)$ is obtained up to second order in $U_0^2$. Toward this end, we consider $k_y = 0$. Equation (5) gives us $C_{\mathbf{k}_\alpha}^{(1)} = C_{\mathbf{k}_\beta}^{(1)} =$

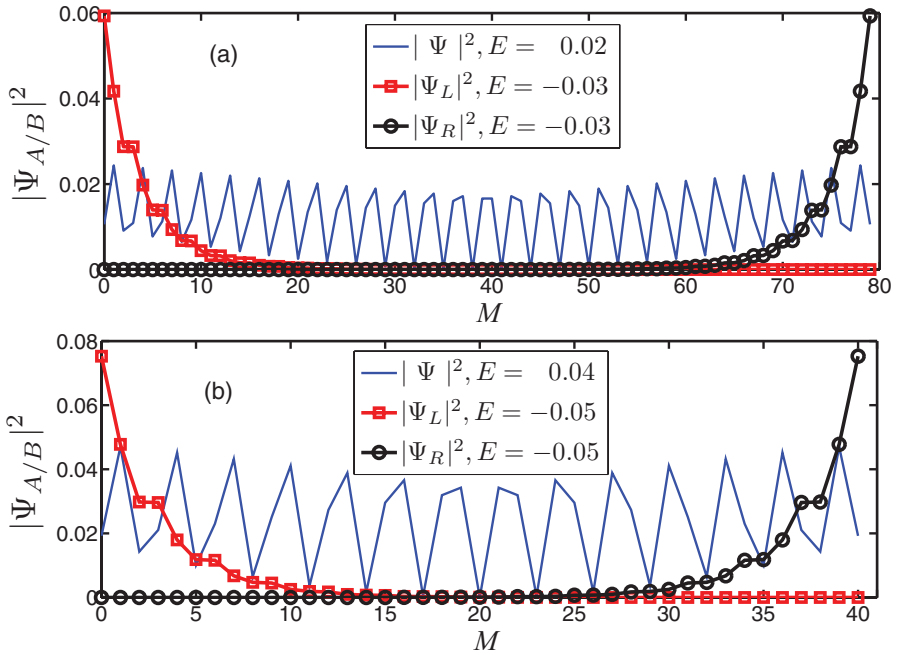


FIG. 6. (Color online) Wave-function spatial profiles for selected energies on the edge-state branches in Fig. 5. $W = 80$ in (a) and 41 in (b). Energies outside (inside) the gray areas in Fig. 5 exhibit edgelike (bulklike) profiles, denoted by squares and circles (solid curves). $\Psi_{R\,(L)}$ denote wave functions that localize on the right (left) edges.

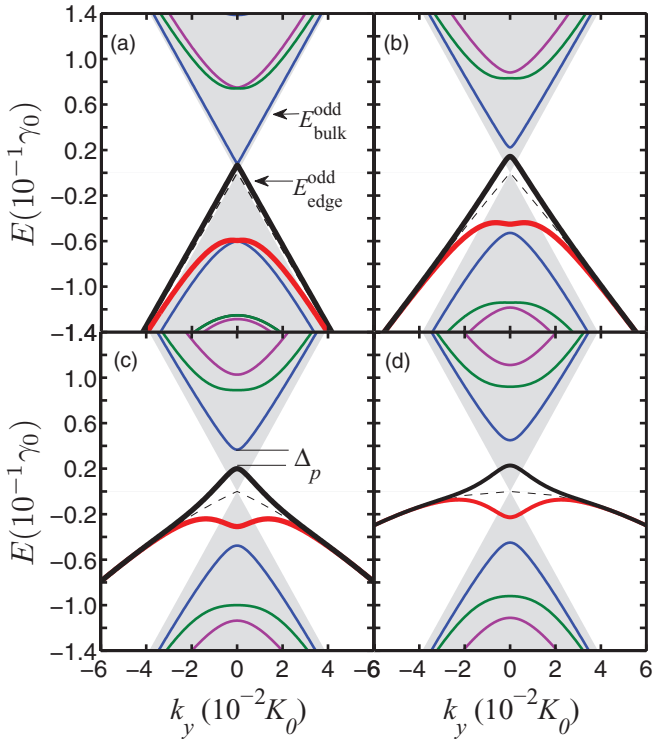


FIG. 7. (Color online) Energy spectrum of the $W = 80$ armchair GNR in Fig. 5. $U_0 = 0.2$, 0.5, 0.8, and 1.0 in (a), (b), (c), and (d), respectively. Near the Dirac cone, the GNR subband ($E^{odd}_{bulk}$) and the edge-state branch ($E^{odd}_{edge}$) are both of odd parity, as denoted in (a). The $U_0$-induced energy gap $\Delta_p$ is indicated in (c). Dotted curve is the open-boundary edge-state branch.

$C^{(1)}_{\mathbf{k}_\gamma} = 1/\sqrt{2}$, $C^{(2)}_{\mathbf{k}_\alpha} = C^{(2)}_{\mathbf{k}_\beta} = -\xi\eta/\sqrt{2}$, and $C^{(2)}_{\mathbf{k}_\gamma} = -C^{(2)}_{\mathbf{k}_\alpha}$ for $\alpha = (\xi,\eta)$. Substituting these into Eq. (26), we obtain $r_{2\alpha} = 0$ and

$$r_{1\alpha} = -\frac{e^{-ik_{\alpha x}M_w a/2}[-U_0\,\xi\eta + e^{-ik_{\alpha x}a_{2x}}]}{e^{ik_{\alpha x}M_w a/2}[-U_0\,\xi\eta + e^{ik_{\alpha x}a_{2x}}]}. \tag{27}$$

Energies for the odd-parity states are determined from Eq. (25), which in turns gives the equation $1 + r_{1\alpha} = 0$. For our purposes here, the unperturbed wave vector $k_x$ for these states is at $\eta K$ when $U_0 = 0$. Keeping up to the second order in $U_0$, the correction $\delta k_{\alpha x}$ is,

$$\begin{aligned}\delta k_{\alpha x} &= \xi\Gamma_1 U_0 + \eta\Gamma_2 U_0^2\\ \Gamma_1 &= -\frac{1}{\sqrt{3}\,(p+1)},\\ \Gamma_2 &= \frac{1}{\sqrt{3}}\left[\frac{1}{2\,(p+1)} - \frac{1}{3(p+1)^2}\right].\end{aligned} \tag{28}$$

The energy shift $\delta E_\alpha$, up to second order in $\delta k_x$, is obtained from Eq. (6), given by

$$\delta E_\alpha = -\xi\left(\sqrt{3}\,\delta k_{x,\alpha} - \tfrac{1}{2}\eta\,\delta k_{\alpha x}^2\right). \tag{29}$$

Substituting Eq. (28) into Eq. (29), the band edges of the subband $E^{odd}_{bulk}$, where $\eta = -1$, and the edge-state branch $E^{odd}_{ed}$, where $\eta = 1$, are obtained as

$$\delta E_\alpha = \left[\frac{1}{(p+1)}U_0 - \xi\eta\frac{p}{2(p+1)^2}U_0^2\right]. \tag{30}$$

Here $\xi = 1$. Finally, the energy gap $\Delta_p$, up to second order in $U_0$, is obtained as

$$\Delta_p = E^{odd}_{bulk}(0) - E^{odd}_{ed}(0) = \frac{p}{(p+1)^2}U_0^2. \tag{31}$$

## IV. CONDUCTANCE OF AN ARMCHAIR GNR

In this section, we present the conductance $G$ of an armchair GNR and its dependences on the edge potential $U_0$ and the chemical potential $\mu$ of the GNR. Our major interest here is to identify the signatures of the edge states and the gap opening in the $G(U_0,\mu)$ characteristics. The Landauer-Büttiker formula[57,58] is used for the calculation of $G$.

Figure 8 shows the contour plot of $G$, where its value, in units of $2e^2/h$, is depicted by integers in the respective regions in the $\mu$-$U_0$ plane. Essentially the integers denote the number of propagating (right-going) channels in the GNR. The $G = 0$ (black) region indicates the energy gap in $\mu$, which has a zero $\mu$ interval at $U_0$ and opens up monotonically with $U_0$. The $\mu$ interval in the small $U_0$ regime is described by Eq. (31). Furthermore, the $U_0 = 0$ results can be understood by comparing the energy spectrum close to that in Fig. 7(a). Increasing $\mu$ from zero, there are two right-going channels, one from each Dirac cone, at $k_y = 0$ and $k_y = \sqrt{3}\,K_0/2$, giving $G = 2$. As $\mu$ increases further, approaching 0.07, two higher GNR subbands enter for each Dirac cone, and $G = 6$. On the other hand, decreasing $\mu$ from zero, the higher GNR subbands enter in a pair for each Dirac cone, and $G$'s value is in the sequence 2, 6, and 8.

Similarly, the trend for finite $U_0$ can be understood from the energy spectrum for $U_0 = 1$, as shown in Fig. 7(d). A few

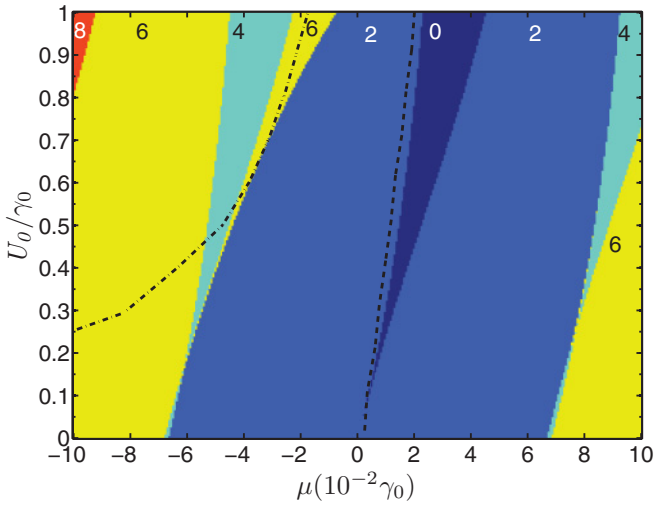


FIG. 8. (Color online) Dependences of conductance on the edge potential $U_0$ and the chemical potential $\mu$. The armchair GNR has $W = 80$. Integers in the figure denote the conductance $G$, in units of $2e^2/h$, in the respective region. Dotted (dotted-dashed) line depicts the odd- (even-) parity edge-state branch that emerges from the continuum spectrum of the bulk graphene.

added features should be noted here. Higher GNR subbands are split and no longer enter in a pair as $\mu$ changes. The energy gap ($G = 0$) is shifted to the positive-$\mu$ region, and the splitting of the edge-state branches near a Dirac cone brings about interesting $G$ structures. The conditions under which the edge-state branches emerge from the continuum spectrum are indicated by the dotted and dot-dashed lines. Thus increasing $\mu$ from zero, the $G$ values are in the sequence 2, 0, 2, and 4. In the opposite direction, when $\mu$ decreases from zero, the sequence of $G$ values becomes 2, 6, 4, 6, and 8. In between the dotted and the dot-dashed lines, where $G = 2$ and 6, the edge states, including both coupled and decoupled edge states, are the sole contributors to $G$. The jump from $G = 2$ to 6 arises from two (one) channels in the even- (odd-) parity edge-state branch, per Dirac cone. The next region ($G = 4$) is another region where $G$ is contributed from edge states alone. Here, however, only decoupled edge states are involved. The characteristics presented above remain intact for the edge potential with a smooth spatial profile.[59] It is perhaps not unexpected that the atomic-scale profile for the edge potential is not very crucial for the features found in this work. It may be that it is the intravalley (small momentum change) scattering, rather than the intervalley (large momentum change) scattering, that must be invoked here. Finally, the edge-state features are expected to be robust against weak disorder due to their chiral nature.

## V. CONCLUSIONS

In conclusion, we have studied the effects of edge potentials on an armchair graphene open boundary, and on armchair GNRs. The connection of the formation of the edge states with the edge-potential-induced pseudospin flipping at the open boundary has been elucidated. The subsequent generation of out-of-plane pseudospin polarizations at an open boundary is demonstrated. In the case of an armchair GNR, both the formation of edge states and the opening of an energy gap are found. These effects exhibit distinct characteristics in the conductance of the GNR. Finally, the edge-potential configuration considered in this work could be realized with the technique of anisotropic etching of graphene by thermally activated nickel nanoparticles,[52] with some of the etched graphene functioning as gating electrodes and others as the GNR.

## ACKNOWLEDGMENTS

We acknowledge useful discussions with M. Monteverde, and we are grateful to him for referring us to Ref. 51. This work was supported by Taiwan NSC (Contract No. 100-2112-M-009-019), NCTS Taiwan, and a MOE-ATU grant.

[1] K. S. Novoselov, A. K. Geim, S. V. Morozov, D. Jiang, Y. Zhang, S. V. Dubonos, I. V. Grigorieva, and A. A. Firsov, Science **306**, 666 (2004).
[2] K. S. Novoselov, D. Jiang, F. Schedin, T. J. Booth, V. V. Khotkevich, S. V. Morozov, and A. K. Geim, Proc. Natl. Acad. Sci. USA **102**, 10451 (2005).
[3] A. K. Geim and K. S. Novoselov, Nat. Mater. **6**, 183 (2007).
[4] C. W. J. Beenakker, Rev. Mod. Phys. **80**, 1337 (2008).
[5] A. H. Castro Neto, F. Guinea, N. M. R. Peres, K. S. Novoselov, and A. K. Geim, Rev. Mod. Phys. **81**, 109 (2009).
[6] N. M. R. Peres and R. M. Ribeiro, New J. Phys. **11**, 095002 (2009).
[7] D. Abergel, V. Apalkov, J. Berashevich, K. Ziegler, and T. Charkraborty, Adv. Phys. **59**, 261 (2010).
[8] S. DasSarma, S. Adam, E. H. Hwang, and E. Ross, Rev. Mod. Phys. **83**, 407 (2011).
[9] P. Avouris, Z. Chen, and V. Perebeinos, Nat. Nanotech. **2**, 605 (2007).
[10] F. Miao, S. Wijeratne, Y. Zhang, U. C. Coskun, W. Bao, and C. N. Lau, Science **317**, 1530 (2007).
[11] L. A. Ponomarenko, F. Schedin, M. I. Katsnelson, R. Yang, E. W. Hill, K. S. Novoselov, and A. K. Geim, Science **320**, 356 (2008).
[12] F. Schwierz, Nat. Nanotech. **5**, 487 (2010).
[13] Y. W. Son, M. L. Cohen, and S. G. Louie, Nature (London) **444**, 347 (2006).
[14] X. Wang, Y. Ouyang, X. Li, H. Wang, J. Guo, and H. Dai, Phys. Rev. Lett. **100**, 206803 (2008).
[15] M. I. Katsnelson, K. S. Novoselov, and A. K. Geim, Nat. Phys. **2**, 620 (2006).
[16] K. I. Bolotin, K. J. Sikes, Z. Jiang, M. Klima, G. Fudenberg, J. Hone, P. Kim, and H. L. Stormer, Solid State Commun. **146**, 351 (2008).
[17] A. A. Balandin, S. Ghosh, W. Z. Bao, I. Calizo, D. Teweldebrhan, F. Miao, and C. N. Lau, Nano Lett. **8**, 902 (2008).
[18] C. H. Park, Y. W. Son, L. Yang, M. L. Cohen, and S. G. Louie, Nano Lett. **8**, 2920 (2008).
[19] L. Majidi and M. Zareyan, Phys. Rev. B **83**, 115422 (2011).
[20] M. Mecklenburg and B. C. Regan, Phys. Rev. Lett. **106**, 116803 (2011).
[21] A. Rycerz, J. Tworzydło, and C. W. J. Beenakker, Nat. Phys. **3**, 172 (2007).
[22] J. L. Garcia-Pomar, A. Cortijo, and M. Nieto-Vesperinas, Phys. Rev. Lett. **100**, 236801 (2008).
[23] D. Gunlycke and C. T. White, Phys. Rev. Lett. **106**, 136806 (2011).
[24] A. F. Young and P. Kim, Nat. Phys. **5**, 222 (2009).
[25] N. Stander, B. Huard, and D. Goldhaber-Gordon, Phys. Rev. Lett. **102**, 026807 (2009).
[26] K. S. Novoselov, A. K. Geim, S. V. Morozov, D. Jiang, M. I. Katsnelson, I. V. Grigorieva, S. V. Dubonos, and A. A. Firsov, Nature (London) **438**, 197 (2005).
[27] Y. Zhang, J. W. Tan, H. L. Stormer, and P. Kim, Nature (London) **438**, 201 (2005).
[28] H. Suzuura and T. Ando, Phys. Rev. Lett. **89**, 266603 (2002).
[29] E. McCann, K. Kechedzhi, V. I. Fal'ko, H. Suzuura, T. Ando, and B. L. Altshuler, Phys. Rev. Lett. **97**, 146805 (2006).
[30] A. F. Morpurgo and F. Guinea, Phys. Rev. Lett. **97**, 196804 (2006).
[31] V. V. Chelanov, V. Fal'ko, and B. L. Altshuler, Science **315**, 1252 (2007).
[32] S. E. Stein and R. L. Brown, J. Am. Chem. Soc. **109**, 3721 (1987).
[33] M. Fujita, K. Wakabayashi, K. Nakada, and K. Kusakabe, J. Phys. Soc. Jpn. **65**, 1920 (1996).

[34]K. Nakada, M. Fujita, G. Dresselhaus, and M. S. Dresselhaus, Phys. Rev. B **54**, 17954 (1996).
[35]S. Ryu and Y. Hatsugai, Phys. Rev. Lett. **89**, 077002 (2002).
[36]T. Hikihara, X. Hu, H. H. Lin, and C. Y. Mou, Phys. Rev. B **68**, 035432 (2003).
[37]C. L. Kane and E. J. Mele, Phys. Rev. Lett. **95**, 226801 (2005).
[38]M. Ezawa, Phys. Rev. B **73**, 045432 (2006).
[39]L. Brey and H. A. Fertig, Phys. Rev. B **73**, 235411 (2006).
[40]N. M. R. Peres, A. H. Castro Neto, and F. Guinea, Phys. Rev. B **73**, 195411 (2006).
[41]N. M. R. Peres, F. Guinea, and A. H. Castro Neto, Phys. Rev. B **73**, 125411 (2006).
[42]C. Ritter, S. S. Makler, and A. Latgé, Phys. Rev. B **77**, 195443 (2008).
[43]W. Yao, S. A. Yang, and Q. Niu, Phys. Rev. Lett. **102**, 096801 (2009).
[44]K. Wakabayashi, S. Okada, R. Tomita, S. Fujimoto, and Y. Natsume, J. Phys. Soc. Jpn. **79**, 034706 (2010).
[45]S. Bhowmick and V. B. Shenoy, Phys. Rev. B **82**, 155448 (2010).
[46]K. Wakabayashi, K. Sasaki, T. Nakanishi, and T. Enoki, Sci. Technol. Adv. Mater. **11**, 054504 (2010).
[47]W. Apel, G. Pal, and L. Schweitzer, Phys. Rev. B **83**, 125431 (2011).
[48]C. Tao, L. Jiao, O. V. Yazyev, Y. C. Chen, J. Feng, X. Zhang, R. B. Capaz, J. M. Tour, A. Zettl, S. G. Louie, H. Dai, and M. F. Crommie, Nat. Phys. **7**, 616 (2011).
[49]P. Delplace, D. Ullmo, and G. Montambaux, Phys. Rev. B **84**, 195452 (2011).
[50]J. Wurm, K. Richter, and I. Adagideli, Phys. Rev. B **84**, 075468 (2011).
[51]X. Jia, M. Hofmann, V. Meunier, B. G. Sumpter, J. Campos-Delgado, J. M. Romo-Herrera, H. Son, Y. P. Hsieh, A. Reina, J. Kong, M. Terrones, and M. S. Dresselhaus, Science **323**, 1701 (2009).
[52]L. C. Campos, V. R. Manfrinato, J. D. Sanchez-Yamagishi, J. Kong, and P. Jarillo-Herrero, Nano Lett. **9**, 2600 (2009).
[53]I. Martin, Y. M. Blanter, and A. F. Morpurgo, Phys. Rev. Lett. **100**, 036804 (2008).
[54]Edge states were obtained in recent work (Ref. 44) on the chemical modification of an armchair edge into a Klein edge, and with a finite transfer integral between Klein's bonds and the armchair edge.
[55]I. Tamm, Phys. Z. Sowjetunion **1**, 733 (1932).
[56]Y. W. Son, M. L. Cohen, and S. G. Louie, Phys. Rev. Lett. **97**, 216803 (2006).
[57]R. Landauer, Philos. Mag. **21**, 863 (1970).
[58]M. Buttiker, Phys. Rev. Lett. **57**, 1761 (1986).
[59]C. H. Chiu and C. S. Chu (unpublished).